

Berry curvature dipole current in transition metal dichalcogenides family

Jih-Shih You,^{1,2,*} Shiang Fang,^{1,†} Su-Yang Xu,³ Efthimios Kaxiras,^{1,4} and Tony Low^{5,‡}

¹*Department of Physics, Harvard University, Cambridge, Massachusetts 02138, USA*

²*Institute for Theoretical Solid State Physics, IFW Dresden, Helmholtzstr. 20, 01069 Dresden, Germany*

³*Department of Physics, Massachusetts Institute of Technology, Cambridge, Massachusetts 02139, USA*

⁴*John A. Paulson School of Engineering and Applied Sciences, Harvard University, Cambridge, Massachusetts 02138, USA*

⁵*Department of Electrical and Computer Engineering, University of Minnesota, Minneapolis, Minnesota 55455, USA*

(Dated: April 7, 2024)

We study the quantum nonlinear Hall effect in two-dimensional materials with time-reversal symmetry. When only one mirror line exists, a transverse charge current occurs in second-order response to an external electric field, as a result of the Berry curvature dipole in momentum space. Candidate 2D materials to observe this effect are two-dimensional transition-metal dichalcogenides (TMDCs). First we use an *ab initio* based tight-binding approach to demonstrate that monolayer T_d -structure TMDCs exhibit a finite Berry curvature dipole. In the $1H$ and $1T'$ phase of TMDCs, we show the emergence of finite Berry curvature dipole with the application of strain and electrical displacement field respectively.

TMDCs¹⁻⁴ have lately attracted considerable attention because of their rich physics, such as charge density wave⁵⁻⁷, superconducting phase⁸, two dimensional (2D) quantum spin Hall (QSH) state⁹⁻¹³ and Weyl semimetal states¹⁴, among other phenomena. Recently numerous studies have demonstrated new physical properties in a monolayer (ML) of TMDCs that may be different from those in bulk. For example, molybdenum disulfide (MoS₂) exhibits an induced indirect to direct band-gap transition from $2H$ -structure to its ML $1H$ -structure, together with an enhancement of the luminescence quantum yield in comparison with the MoS₂ bulk^{15,16}. The $1H$ -structure which does not possess a center of inversion, in contrast to the $2H$ -structure, allows optical control of valley degrees of freedom¹⁷.

Generally, the electronic properties of monolayer TMDCs with chemical composition MX₂ (M = Mo, W; and X = S, Se, Te) are directly related to their crystal structure, which includes the $1H$ ($P\bar{6}m2$), $1T$ ($P\bar{3}m2$), $1T'$ ($P2_1/m$), and T_d ($P1m1$) crystal structures, shown in Fig. 1. $1H$ - MX₂ is a semiconductor with a direct band gap in the range of visible light (1 to 2 eV)^{1,18,19} and the $1T$ structure is metallic²⁰. Topological phases occur in $1T'$ structures since the global properties of electronic wavefunctions exhibit a non-trivial topology, theoretically predicted⁹ and experimentally confirmed¹⁰⁻¹³ to be a 2D quantum spin Hall state.

The local curvature of the wavefunction, defined as the Berry curvature (BC)^{21,22}, is a geometrical property of the Bloch energy band. The finite Berry curvature reveals linear response, such as anomalous Hall conductivity²¹, and nonlinear response, such as circular photogalvanic effect (CPGE) and nonlinear Hall effect²³⁻³⁴. In TMDCs, the BC at the two valleys takes opposite values, giving rise to bulk topological charge neutral valley current³⁵⁻³⁷, as a linear response. For nonlinear response, the semiclassical approach has been used to describe the intra-band contributions to transverse current at both

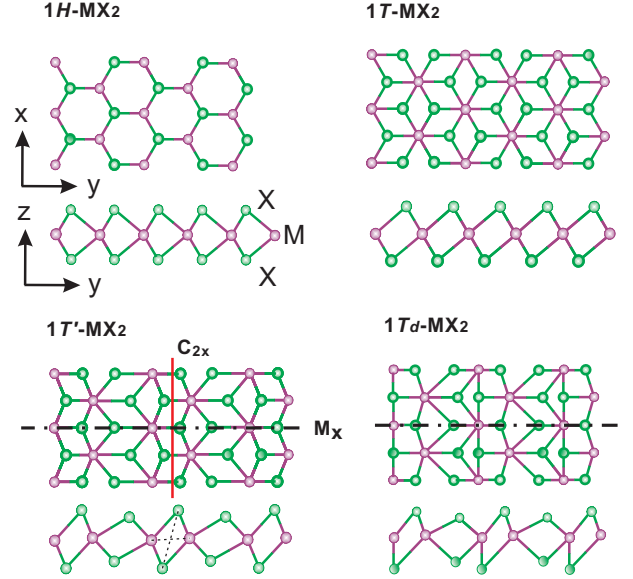


FIG. 1. Crystal structures of $1H$, $1T$, $1T'$ and $1T_d$ monolayer transition metal dichalcogenides MX₂ (M = Mo, W and X = S, Se, Te). The red solid line represents a screw rotate symmetry C_{2x} axis which involves a 180° rotation about \hat{x} and a half lattice-constant translation along \hat{x} . The dashed-dotted line represents the mirror symmetry M_x . The combination of C_{2x} and M_x symmetries leads to the inversion symmetry for the $1T'$ structure. The $1T_d$ phase has only M_x symmetry.

zero frequency and second harmonic generation in terms of the dipole moment of the BC in momentum space²⁶. In the dc limit, the photocurrent can remain finite as a transverse Hall-like current^{26,32}.

In this work, we study the emergence of the non-linear Hall current induced by the BC dipole in various 2D TMDC structures, using *ab initio* calculations combined with a semiclassical approach. Monolayer TMDCs with low crystalline symmetry are expected to be excellent

candidates for observing these quantum non-linear effects²⁶. Our study quantitatively reveals the finite BC dipole in the T_d -structure monolayer TMDCs, where only one mirror line survives. For the $1H$ structure, uniaxial strain can break the underlying C_{3v} symmetry which otherwise ensures vanishing nonlinear response. In addition, we evaluate the Berry dipole of strained TMDC. Lastly, we show that application of an out-of-plane electrical displacement field induces a strong BC dipole which is absent in $1T'$ monolayer TMDCs. Our results represent the first numerical demonstration of non-linear current in 2D TMDCs, which can be controlled by mechanical and/or electrical means. The proposed strategies of a tunable BC dipole also apply to a wide range of other two dimensional materials, such as hexagonal boron nitride³⁸ and black phosphorus³⁹⁻⁴¹.

In the presence of an external electric field, the carrier velocity contains contributions from the group velocity of the electron wave and from the anomalous transverse term due to the BC, given by $-\frac{e}{\hbar}\vec{E} \times \Omega_z^{(n)}(\vec{k})$. Here the BC for the electronic Bloch states of the n th band is defined as^{22,42,43}

$$\begin{aligned} \Omega_z^{(n)}(\vec{k}) &= i\hat{z} \cdot (\nabla_{\vec{k}} u_{\vec{k}}^{(n)*}) \times (\nabla_{\vec{k}} u_{\vec{k}}^{(n)}) \\ &= -2\left(\frac{\hbar}{e}\right)^2 \sum_{n \neq n'} \frac{\text{Im}\langle u_{\vec{k}}^{(n)} | P_x(\vec{k}) | u_{\vec{k}}^{(n')} \rangle \langle u_{\vec{k}}^{(n')} | P_y(\vec{k}) | u_{\vec{k}}^{(n)} \rangle}{[\epsilon_{\vec{k}}^{(n)} - \epsilon_{\vec{k}}^{(n')}]^2} \end{aligned} \quad (1)$$

where $\epsilon_{\vec{k}}^{(n)}$ and $|u_{\vec{k}}^{(n)}\rangle$ are eigenvalues and eigenfunctions of the Hamiltonian $\hat{H}_{\vec{k}}$, respectively, at the momentum \vec{k} and $P_i(\vec{k}) = (e/\hbar)\partial\hat{H}_{\vec{k}}/\partial k_i$ is the current operator. The BC is analogous to an effective magnetic field in the momentum space. Within linear response theory, the integral of the BC over the entire Brillouin zone gives rise to a transverse conductivity, which is simply given by $\sigma_{xy,n} = e^2/\hbar \int d^2\vec{k} f_0^{(n)}(\vec{k}) \Omega_z^{(n)}(\vec{k})$, where $f_0^{(n)}(\vec{k})$ is the equilibrium Fermi-Dirac distribution function for n th band. The transverse conductivity is zero for a time-reversal-invariant system, since states at \vec{k} and $-\vec{k}$ are equally occupied and time-reversal symmetry requires that $\Omega_z^{(n)}(\vec{k}) = -\Omega_z^{(n)}(-\vec{k})$. When the system is driven out-of-equilibrium, a net transverse current can survive as the second order response to the electric field. The combination of time reversal (TR) and inversion symmetry restricts $\Omega_z^{(n)}(\vec{k}) = 0$ over the entire Brillouin zone. Thus, for a TR invariant system, inversion symmetry breaking is necessary to generate a finite BC.

We first examine the nature of the non-linear current with a symmetry analysis. In the presence of a driving in-plane electric field, $E_k(t) = \Re\{\mathcal{E}_k e^{i\omega t}\}$, the non-linear current is written as $j_i = j_i^{(0)} + j_i^{(2\omega)} e^{2i\omega t}$, where the dc and second harmonic generated currents are described by the second-order susceptibility tensor as $j_i^{(0)} = \chi_{ijk} \mathcal{E}_j^* \mathcal{E}_k$ and $j_i^{(2\omega)} = \chi_{ijk} \mathcal{E}_j \mathcal{E}_k$, respectively. The tensor indices i, j, k span the 2D sample coordinates x, y . χ_{ijk} respects the symmetry of the crystal lattice. The presence of M_x

mirror symmetry forces χ_{ijk} to be zero if any χ_{ijk} contains an odd number of the index x . All tensor components identically vanish in the presence of inversion symmetry. Thus, for a crystal breaking inversion but preserving the mirror symmetry M_x , $\chi_{yxx} \neq 0$, demonstrating that a Hall-like transverse current can occur in second-order response to an external electric field \mathcal{E}_x .

The expression of nonlinear currents has been theoretically obtained within the semiclassical Boltzmann transport theory for a single band^{25,26}. Up to second order in the driving electric field, previous theoretical works showed that in the case involving only the intra-band process, a nonlinear Hall-like current density is expressed as

$$\vec{j}^{(0)} = \frac{e^3 \tau}{2\hbar^2(1+i\omega\tau)} \hat{z} \times \vec{\mathcal{E}}^* (D \cdot \vec{\mathcal{E}}) \quad (3)$$

$$\vec{j}^{(2\omega)} = \frac{e^3 \tau}{2\hbar^2(1+i\omega\tau)} \hat{z} \times \vec{\mathcal{E}} (D \cdot \vec{\mathcal{E}}) \quad (4)$$

with

$$\begin{aligned} D_i &= \sum_n \int d^2\vec{k} f_0^{(n)}(\vec{k}) [\partial_{k_i} \Omega_z^{(n)}(\vec{k})] \\ &= - \sum_n \int d^2\vec{k} [\partial_{k_i} f_0^{(n)}(\vec{k})] \Omega_z^{(n)}(\vec{k}) \end{aligned} \quad (5)$$

where τ is the relaxation time. The nonlinear dc current is proportional to the dipole moment of the BC over the occupied states. In fact, according to Eq. (5) the non-linearity of these currents is associated with a ‘‘Fermi-surface’’ contribution, that is, only states near the Fermi surface can contribute to the integral in the low temperature limit. The largest symmetry of a 2D crystal that allows for a non-vanishing BC dipole is a single mirror line²⁶. Combining Eq. (5) with the fact that $\Omega_z^{(n)}(k_x, k_y) = -\Omega_z^{(n)}(-k_x, k_y)$ enforced by the mirror plane M_x , it is evident that $D_x \neq 0$ and $D_y = 0$. Consequently, according to Eq.s (3) and (4), when the driving electric field $E_k(t) = \mathcal{E}_k$ is aligned with the direction of the Berry curvature dipole vector D_x , we obtain the dc current density $j = 2j^{(0)} = 3698.1(A/m^2) \times D_x \sim 10^{-7}(A/m)$, where we choose $\tau = 10^{-12}s$, $D_x = 1\text{\AA}$ and $\mathcal{E}_x = 100V/m$.

The BC dipole is tied to the underlying crystal structure of monolayer TMDC. The most studied polymorphic structures of pristine monolayer TMDCs are $1H$, $1T$, and $1T'$ ^{44,45}, shown in Fig. 1. The energetically favorable $1H - MX_2$ layer is built from two hexagonal lattices of X atoms and an intercalated hexagonal plane of M atoms forming a simple ABA Bernal stacking with $P\bar{6}m2$ space-group symmetry. In a monolayer unit of H structure, the inversion symmetry is explicitly broken. The lack of an inversion center in TMDCs produces substantial local BCs near the K, K' valleys. Due to time-reversal symmetry, the curvature at the two valleys has opposite sign, which implies counter-propagating currents that persist even when the system is in equilibrium. Due to exact cancellation from the two valleys, these transverse currents

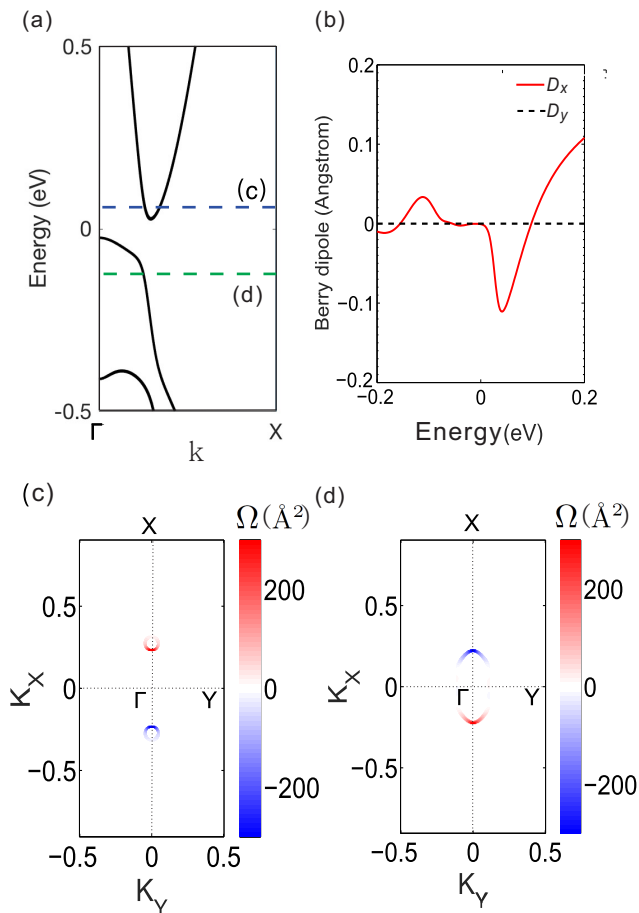


FIG. 2. (a) Band structure along Γ -X for the monolayer T_d -structure WTe_2 . The global band gap is around 0.05 eV. The weak inversion breaking induces a tiny spin splitting near the bottom of the conduction band. The blue and green dashed lines correspond to 0.05 eV and -0.1 eV at which the Berry curvature is shown in (c) and (d), respectively. (b) Berry curvature dipole D_x and D_y . (c) and (d) Berry curvature at 0.05 eV and -0.1 eV, respectively.

are charge neutral to linear response in an applied external electric field. The nonlinear contribution could still exist when the samples have just one mirror symmetry. 2D materials like monolayer TMDCs in the H -structure do not have currents in nonlinear response to the electric field because their C_{3v} symmetry forces the BC dipole to vanish.

The $1T$ - MX_2 layer forms a rhombohedral ABC stacking phase with $P\bar{3}m2$ space group. In this structure, the transition metal atoms are octahedrally coordinated. DFT calculations show that the free-standing $1T$ structure is typically unstable and undergoes Peierls distortion in one direction to form a 2×1 reconstruction, where the distorted M atoms form 1D zigzag chains⁴⁶, referred to as the T' structure. Inversion symmetry is present in both the T - and T' -structure. The inversion-symmetric $1T'$ structure consists of two independent symmetries, the mirror symmetry M_x and the two-fold screw rotational

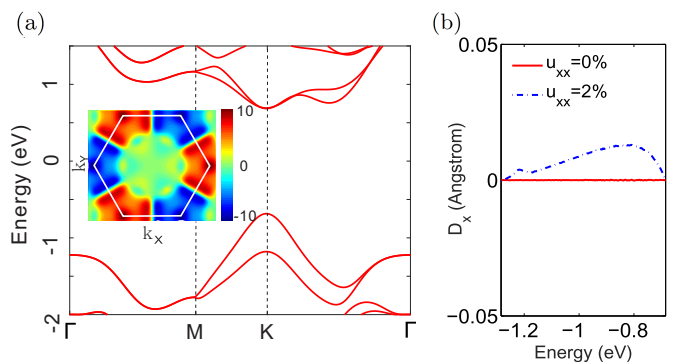


FIG. 3. (a) Band structure along Γ -M-K- Γ for the strained H -structure WSe_2 ; the inset shows the Berry curvature contributed from the top two valance bands. The Brillouin zone is presented in white solid line. (b) Berry curvature dipole D_x of the monolayer H -structure WSe_2 with strain $u_{xx} = 0$ (red line) and $u_{xx} = 2\%$ (blue dotted line) when $u_{yy} = u_{xy} = 0$. $D_y = 0$ for all strains.

symmetry C_{2x} . Due to the inversion symmetry and time-reversal symmetry, $\Omega_z^{(n)}(\vec{k}) = 0$ over the entire Brillouin zone for the $1T'$ -structure.

A candidate material to observe the quantum nonlinear Hall effect is monolayer WTe_2 , whose structure T_d deviates slightly from the widely-studied $1T'$ structure. In the T_d phase, the M_x mirror symmetry is preserved but the C_{2x} symmetry is weakly broken. As a result, the T_d structure with symmetry space group $P1m1$ actually breaks inversion symmetry and allows a non-zero BC dipole to exist. We perform *ab initio* density-functional theory (DFT) calculations using the Vienna *Ab initio* Simulation Package (VASP)^{47,48} with a minimal basis based on a transformation of the Kohn-Sham density functional theory Hamiltonian to a basis of maximally localized Wannier functions⁴⁹ as implemented in the Wannier90 code. A slab geometry is employed to model single or double layers with a 20\AA vacuum region between periodic images to minimize the interaction between slabs. For TMDC materials, the relevant states consist of seven valence bands and four conduction bands, which are hybrids of metal d orbitals and chalcogen p orbitals. Therefore, the Wannier projections to the p/d orbitals provides us the *ab initio* tight-binding Hamiltonian for computing the BC dipole^{50,51}.

In Fig. 2 we shows that the ML WTe_2 with spin-orbit coupling (SOC) exhibits a finite BC dipole. The SOC leads to an inverted, indirect quantum spin Hall gap. In the DFT calculation, we used the Heyd-Scuseria-Ernzerhof (HSE) method⁵² with the hybrid parameter set at HSE= 0.4, which gives a global band gap of 50 meV. In the vicinity of the gap minimum, the BC for the lowest conduction band exhibits two hotspots of opposite sign, as shown in Fig. 2(c). Such bipolar configuration of BC is due to the M_x symmetry. It is worth noting that the distribution of BC near each hotspot is not uniform, leading to a nonzero BC dipole. To

better understand the physics, we rewrite Eq. (5) as $D_x = \sum_n \int d^2k \delta(\epsilon_{\vec{k}}^{(n)} - E_F) [\partial_{k_x} \epsilon_{\vec{k}}^{(n)}] \Omega_z^{(n)}(\vec{k})$, where E_F is the Fermi energy and $\partial_{k_x} \epsilon_{\vec{k}}^{(n)}$ is associated with the velocity along x -direction. Let us first consider the case of one Dirac cone (one hotspot). If the BC is constant and the velocity is equal but opposite around a perfect Dirac cone, the BC dipole will vanish. However, for a tilted Dirac cone which has anisotropic BC and velocity around E_F , a finite BC dipole is allowed. In Fig. 2 (c), the red (blue) hotspot shows more intense positive (negative) BC in the left (right) part of the Dirac cone, where the velocity is negative (positive) along x -direction, leading to a negative BC dipole. For the highest valance band, the slope is negative along Γ to X , as shown in Fig. 2 (a). Thus, the configuration of BC in Fig. 2 (d) gives a positive BC dipole.

The H -structure monolayer TMDCs do not have nonlinear currents due to their C_{3v} symmetry, but applying uniaxial strain can reduce this symmetry and leaving only a single mirror operation, in which case the quantum non-linear Hall effect can be observed²⁶. The application of strain transforms the vector \vec{r}_0 , which denotes undistorted crystal coordinate, into the new position $\vec{r} = \vec{r}_0 + \vec{u}$, where $\vec{r}_0 = (x, y)$ and $\vec{u} = (u_x(x, y), u_y(x, y))$ are the position and displacement deformation vector field, respectively. Here we are considering only the acoustic part of the in-plane displacement vector. In general, the derivative of \vec{u} can be decomposed as $\vec{\nabla} \vec{u} = \varepsilon + \omega$, where ε and ω are the strain and rotation tensors, respectively.

The simplest way to incorporate the effect of strain is to vary the interatomic bond lengths, $|\delta_{\alpha\beta}|$, between α and β sites, which is known as the central force approximation. At the linear order and under this approximation, the modified hopping terms in the presence of strain can be approximated as

$$t_{\alpha\beta} = t_{\alpha\beta}^0 + \mu \vec{\delta}_{\alpha\beta} \cdot (\vec{\delta}_{\alpha\beta} \cdot \vec{\nabla}) \vec{u}, \mu = \frac{1}{|\delta_{\alpha\beta}|} \left[\frac{dt_{\alpha\beta}}{d|\delta_{\alpha\beta}|} \right]. \quad (6)$$

The central force approximation fails to capture the change in the hopping when the crystal is stretched along a direction perpendicular to the bond. The microscopic models based on the *ab initio* derived Wannier functions describe up to linear order contributions in the strain $(u_{xx} + u_{yy})$, $(u_{xx} - u_{yy})$ and u_{xy} with respect to the crystal symmetry and local crystal configuration, free from any empirical fitting procedures.

Based on the models of strained TMDCs⁵³, the BC dipole can be readily evaluated. Fig. 3 shows that the H -structure WSe₂ with strain exhibits BC dipole. The Brillouin zone of monolayer TMDC with Dirac points is shifted away from the K and K' by uniaxial strain. When the shear strain is applied along high-symmetry lines, one obtains finite D_x but zero D_y .

The application of an out-of-plane electrical displacement field can be used to systematically control the magnitude of the nonlinear Hall current. This can be understood from a third order susceptibility tensor $\chi_{ijjz}^{(3)}$. In

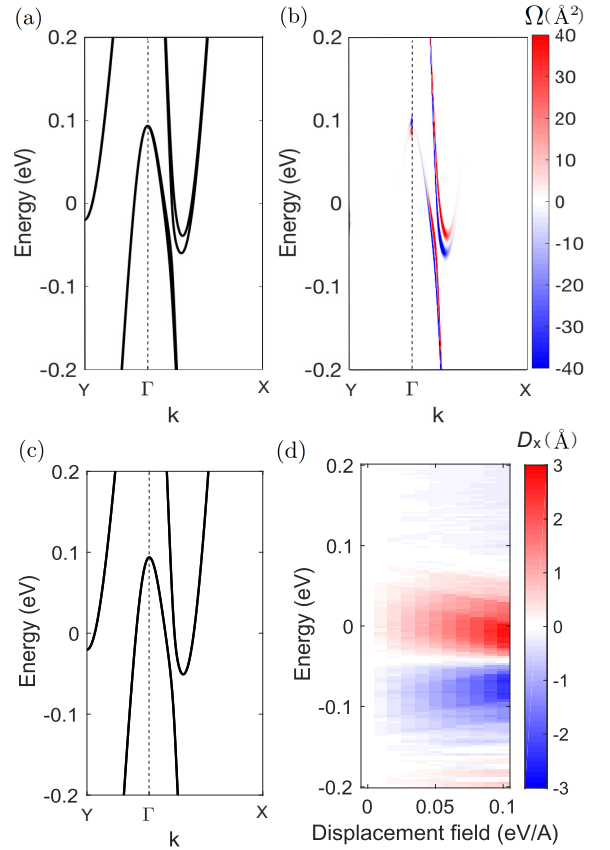


FIG. 4. (a) Band structure and (b) Berry curvature $\Omega_z^{(n)}(\vec{k})$ along $Y-\Gamma-X$ for the ML $1T'$ -structure MoTe₂ at $\mathcal{E}_{d,z} = 0.06$ eV/Å. (c) Band structure at $\mathcal{E}_{d,z} = 0$. The BC is zero at all energies due to the presence of inversion symmetry. (d) BC dipole D_x induced by the electrical displacement field (eV/Å) in the z -direction which breaks the inversion symmetry. $D_y = 0$ in all cases.

the presence of a static electrical displacement field $\mathcal{E}_{d,z}$ along the z -direction the nonlinear dc current is written as $j_i^{(0)} = \chi_{ijj}^{(2)} |\mathcal{E}_j|^2 + \chi_{ijjz}^{(3)} |\mathcal{E}_j|^2 \mathcal{E}_{d,z}$. We obtain the effective second-order tensor containing the electrical displacement field effect as $\tilde{\chi}_{ijj}^{(2)} \equiv \chi_{ijj}^{(2)} + \chi_{ijjz}^{(3)} \mathcal{E}_{d,z}$. When $\chi_{ijj}^{(2)} = 0$ due to the intrinsic inversion symmetry, $\mathcal{E}_{d,z}$ makes it possible to produce the second response with significant amplitude.

Finally we consider the basic symmetry properties of the Hamiltonian for the TMDC family of materials in the presence of $\mathcal{E}_{d,z}$. The $1T'$ phase has inversion symmetry from the combination of two-fold screw rotational symmetry C_{2x} and the mirror symmetry M_x . Therefore the monolayer $1T'$ structure, which has zero BC dipole, can acquire non-zero dipole if $\mathcal{E}_{d,z}$ is applied to break the C_{2x} symmetry and thus inversion symmetry. This inversion symmetry-breaking scheme can be simply modeled with only electrostatic on-site potential within each unit cell. We show the monolayer MoTe₂ with $1T'$ structure as a function of electrical displacement \mathcal{E} -field in the z -

direction in Fig. 4. The enhancement of the BC dipole is evident. This illustrates how to control and modulate the BC dipole with an external field.

In conclusion, we discussed the non-linear current induced by the BC dipole in 2D materials of the TMDC family. The existence of only a single mirror symmetry line is needed to provide a finite BC dipole. Breaking of the crystal symmetry can be controlled by mechanical and/or electrical means. Certainly, it would be desirable to explore the proposed effect could be observed in other 2D materials subject to the same symmetry constraints. Such a tunable BC dipole not only can lead to the quantum nonlinear Hall effect but could also be relevant for the understanding of other quantum geometrical phenomena.

ACKNOWLEDGMENTS

We thank Inti Sodemann, Bertrand I. Halperin, Philip Kim and Jeroen van den Brink for useful discussions. J.-

S.Y. thanks Ulrike Nitzsche for technical assistance. This work was supported by the STC Center for Integrated Quantum Materials, NSF Grant No. DMR-1231319 and by ARO MURI Award W911NF-14-0247. The computations in this paper were run on the Odyssey cluster supported by the FAS Division of Science, Research Computing Group at Harvard University.

Note added: Upon the completion of this manuscript, there appeared an independent work by Yang Zhang *et al.*⁵⁴ which also shows the nonlinear electric response in MoTe₂ and WTe₂ monolayers.

* jihshihyou@gmail.com

† shiangfang913@gmail.com

‡ tlow@umn.edu

- ¹ B. Radisavljevic, A. Radenovic, J. Brivio, V. Giacometti, and A. Kis, *Nature Nanotechnology* **6**, 147 (2011).
- ² Q. H. Wang, K. Kalantar-Zadeh, A. Kis, J. N. Coleman, and M. S. Strano, *Nature Nanotechnology* **7**, 699 (2012).
- ³ A. K. Geim and I. V. Grigorieva, *Nature* **499**, 419 (2013).
- ⁴ S. Z. Butler, S. M. Hollen, L. Cao, Y. Cui, J. A. Gupta, H. R. Gutiérrez, T. F. Heinz, S. S. Hong, J. Huang, A. F. Ismach, E. Johnston-Halperin, M. Kuno, V. V. Plashnitsa, R. D. Robinson, R. S. Ruoff, S. Salahuddin, J. Shan, L. Shi, M. G. Spencer, M. Terrones, W. Windl, and J. E. Goldberg, *ACS Nano* **7**, 2898 (2013).
- ⁵ J. A. Wilson, F. J. D. Salvo, and S. Mahajan, *Advances in Physics* **50**, 1171 (2001).
- ⁶ T. Ritschel, J. Trinckauf, K. Koepf, B. Büchner, M. v. Zimmermann, H. Berger, Y. I. Joe, P. Abbamonte, and J. Geck, *Nature Physics* **11**, 328 (2015).
- ⁷ A. W. Tsen, R. Hovden, D. Wang, Y. D. Kim, J. Okamoto, K. A. Spoth, Y. Liu, W. Lu, Y. Sun, J. C. Hone, L. F. Kourkoutis, P. Kim, and A. N. Pasupathy, *Proceedings of the National Academy of Sciences* **112**, 15054 (2015).
- ⁸ J. T. Ye, Y. J. Zhang, R. Akashi, M. S. Bahramy, R. Arita, and Y. Iwasa, *Science* **338**, 1193 (2012).
- ⁹ X. Qian, J. Liu, L. Fu, and J. Li, *Science* **346**, 1344 (2014).
- ¹⁰ Z. Fei, T. Palomaki, S. Wu, W. Zhao, X. Cai, B. Sun, P. Nguyen, J. Finney, X. Xu, and D. H. Cobden, *Nature Physics* **13**, 677 (2017).
- ¹¹ S. Tang, C. Zhang, D. Wong, Z. Pedramrazi, H.-Z. Tsai, C. Jia, B. Moritz, M. Claassen, H. Ryu, S. Kahn, J. Jiang, H. Yan, M. Hashimoto, D. Lu, R. G. Moore, C.-C. Hwang, C. Hwang, Z. Hussain, Y. Chen, M. M. Ugeda, Z. Liu, X. Xie, T. P. Devereaux, M. F. Crommie, S.-K. Mo, and Z.-X. Shen, *Nature Physics* **13**, 683 (2017).
- ¹² Z.-Y. Jia, Y.-H. Song, X.-B. Li, K. Ran, P. Lu, H.-J. Zheng,

- X.-Y. Zhu, Z.-Q. Shi, J. Sun, J. Wen, D. Xing, and S.-C. Li, *Physical Review B* **96**, 041108 (2017).
- ¹³ S. Wu, V. Fatemi, Q. D. Gibson, K. Watanabe, T. Taniguchi, R. J. Cava, and P. Jarillo-Herrero, *Science* **359**, 76 (2018).
- ¹⁴ A. A. Soluyanov, D. Gresch, Z. Wang, Q. Wu, M. Troyer, X. Dai, and B. A. Bernevig, *Nature* **527**, 495 (2015).
- ¹⁵ A. Splendiani, L. Sun, Y. Zhang, T. Li, J. Kim, C.-Y. Chim, G. Galli, and F. Wang, *Nano Letters* **10**, 1271 (2010).
- ¹⁶ K. F. Mak, C. Lee, J. Hone, J. Shan, and T. F. Heinz, *Physical Review Letters* **105**, 136805 (2010).
- ¹⁷ H. Zeng, J. Dai, W. Yao, D. Xiao, and X. Cui, *Nature Nanotechnology* **7**, 490 (2012).
- ¹⁸ X. R. Qin, D. Yang, R. F. Frindt, and J. C. Irwin, *Physical Review B* **44**, 3490 (1991).
- ¹⁹ S. Fang, R. K. Defo, S. N. Shirodkar, S. Lieu, G. A. Tritsarolis, and E. Kaxiras, *Physical Review B* **92**, 205108 (2015).
- ²⁰ R. Kappera, D. Voiry, S. E. Yalcin, W. Jen, M. Acerce, S. Torrel, B. Branch, S. Lei, W. Chen, S. Najmaei, J. Lou, P. M. Ajayan, G. Gupta, A. D. Mohite, and M. Chhowalla, *APL Materials* **2**, 092516 (2014).
- ²¹ N. Nagaosa, J. Sinova, S. Onoda, A. H. MacDonald, and N. P. Ong, *Reviews of Modern Physics* **82**, 1539 (2010).
- ²² D. Xiao, M.-C. Chang, and Q. Niu, *Reviews of Modern Physics* **82**, 1959 (2010).
- ²³ E. Deyo, L. E. Golub, E. L. Ivchenko, and B. Spivak, *arXiv:0904.1917* (2009).
- ²⁴ J. E. Moore and J. Orenstein, *Physical Review Letters* **105**, 026805 (2010).
- ²⁵ T. Low, Y. Jiang, and F. Guinea, *Physical Review B* **92**, 235447 (2015).
- ²⁶ I. Sodemann and L. Fu, *Physical Review Letters* **115**, 216806 (2015).
- ²⁷ M. Eginligil, B. Cao, Z. Wang, X. Shen, C. Cong, J. Shang,

- C. Soci, and T. Yu, *Nature Communications* **6**, 7636 (2015).
- ²⁸ F. de Juan, A. G. Grushin, T. Morimoto, and J. E. Moore, *Nature Communications* **8**, 15995 (2017).
- ²⁹ S. S. Tsirkin, P. A. Puente, and I. Souza, *Physical Review B* **97**, 035158 (2018).
- ³⁰ Y. Zhang, Y. Sun, and B. Yan, *Physical Review B* **97**, 041101 (2018).
- ³¹ J. Quereda, T. S. Ghiasi, J.-S. You, J. van den Brink, B. J. van Wees, and C. H. van der Wal, arXiv:1803.08289 (2018), arXiv:1803.08289 [cond-mat.mtrl-sci].
- ³² S.-Y. Xu, Q. Ma, H. Shen, V. Fatemi, S. Wu, T.-R. Chang, G. Chang, A. M. M. Valdivia, C.-K. Chan, Q. D. Gibson, J. Zhou, Z. Liu, K. Watanabe, T. Taniguchi, H. Lin, R. J. Cava, L. Fu, N. Gedik, and P. Jarillo-Herrero, *Nature Physics* (2018), 10.1038/s41567-018-0189-6.
- ³³ J. I. Facio, D. Efremov, K. Koepernik, J.-S. You, I. Sodemann, and J. van den Brink, ArXiv e-prints (2018), arXiv:1805.02680 [cond-mat.mes-hall].
- ³⁴ L. kun Shi and J. C. W. Song, ArXiv e-prints (2018), arXiv:1805.00939 [cond-mat.mes-hall].
- ³⁵ D. Xiao, G.-B. Liu, W. Feng, X. Xu, and W. Yao, *Physical Review Letters* **108**, 196802 (2012).
- ³⁶ K. F. Mak, K. L. McGill, J. Park, and P. L. McEuen, *Science* **344**, 1489 (2014).
- ³⁷ Y. D. Lensky, J. C. Song, P. Samutpraphoot, and L. S. Levitov, *Physical Review Letters* **114**, 256601 (2015).
- ³⁸ D. Golberg, Y. Bando, Y. Huang, T. Terao, M. Mitome, C. Tang, and C. Zhi, *ACS Nano* **4**, 2979 (2010).
- ³⁹ A. Morita, *Applied Physics A Solids and Surfaces* **39**, 227 (1986).
- ⁴⁰ L. Li, Y. Yu, G. J. Ye, Q. Ge, X. Ou, H. Wu, D. Feng, X. H. Chen, and Y. Zhang, *Nature Nanotechnology* **9**, 372 (2014).
- ⁴¹ H. Liu, A. T. Neal, Z. Zhu, Z. Luo, X. Xu, D. Tománek, and P. D. Ye, *ACS Nano* **8**, 4033 (2014).
- ⁴² J. N. Fuchs, F. Piéchon, M. O. Goerbig, and G. Montambaux, *The European Physical Journal B* **77**, 351 (2010).
- ⁴³ X. Xu, W. Yao, D. Xiao, and T. F. Heinz, *Nature Physics* **10**, 343 (2014).
- ⁴⁴ J. Heising and M. G. Kanatzidis, *Journal of the American Chemical Society* **121**, 11720 (1999).
- ⁴⁵ G. Eda, T. Fujita, H. Yamaguchi, D. Voiry, M. Chen, and M. Chhowalla, *ACS Nano* **6**, 7311 (2012).
- ⁴⁶ M. Kan, J. Y. Wang, X. W. Li, S. H. Zhang, Y. W. Li, Y. Kawazoe, Q. Sun, and P. Jena, *The Journal of Physical Chemistry C* **118**, 1515 (2014).
- ⁴⁷ G. Kresse and J. Furthmüller, *Phys. Rev. B* **54**, 11169 (1996).
- ⁴⁸ G. Kresse and J. Furthmüller, *Computational Materials Science* **6**, 15 (1996).
- ⁴⁹ A. A. Mostofi, J. R. Yates, Y.-S. Lee, I. Souza, D. Vanderbilt, and N. Marzari, *Computer Physics Communications* **178**, 685 (2008).
- ⁵⁰ T. Fukui, Y. Hatsugai, and H. Suzuki, *Journal of the Physical Society of Japan* **74**, 1674 (2005).
- ⁵¹ Based on the tight-binding Hamiltonian, the BC is computed in discretized Brillouin Zone⁵⁰. For the BC dipole, we sample the first Brillouin zone more than 500×500 k-grids.
- ⁵² J. Heyd, G. E. Scuseria, and M. Ernzerhof, *The Journal of Chemical Physics* **118**, 8207 (2003).
- ⁵³ S. Fang, S. Carr, M. A. Cazalilla, and E. Kaxiras, *Physical Review B* **98**, 075106 (2018).
- ⁵⁴ Y. Zhang, J. van den Brink, C. Felser, and B. Yan, ArXiv e-prints (2018), arXiv:1804.11069 [cond-mat.mtrl-sci].